# Incompressible CFD Results Using LS-DYNA. For High Reynolds Number Flow Around Bluff Bodies

Iñaki ÇALDICHOURY (LSTC-AS+),
Facundo DEL PIN(LSTC),
Vincent LAPOUJADE (AS+)

**Abstract**

This report will provide some insight on the new incompressible CFD solver that will be available in version 980 of LS-DYNA. Several test cases were performed by AS+ in order to evaluate the capabilities of these new solvers. These studies were conducted in cooperation with LSTC's CFD developers. Among the various test cases, the airflow over the Ahmed body, a simplified car model will be presented. The flow around this body reproduces the basic aerodynamic features of cars on a well defined basic geometry in order to study the complex interactions associated with vortex wakes and boundary layer separation/reattachment zones. Results were compared to experimental data extracted from reference papers. The results shown here are all part of the global validation process of the incompressible CFD solver.

## Contents

**1 Introduction to the Incompressible CFD solver in LS-DYNA 2**

**2 Flow around the Ahmed body 2**
2.1 Problem description . . . . . 2
2.2 Computational domain . . . . . 3
2.3 Fluid parameters . . . . . 3
2.4 Choice of the turbulence model . . . . . 3
2.4.1 The RANS model . . . . . 3
2.4.2 The LES model . . . . . 6
2.5 Numerical results . . . . . 6
2.5.1 Flow in the near wake . . . . . 6
2.5.2 Drag coefficient . . . . . 7
2.6 Other possible applications of LS-DYNA in the aerodynamics study of bluff bodies . . . . . 8

# 1 Introduction to the Incompressible CFD solver in LS-DYNA

The current development of a incompressible CFD solver in LS-DYNA is focused on flows at low speed where the Mach number $< 0.3$ and whenever the incompressible hypothesis holds. The solver may run as a stand alone CFD solver where only fluid dynamics effects are studied or it could be coupled to the solid mechanics solver to study fluid-structure interaction (FSI) problems.

Some of the features of the solver include an embedded volume mesher. This could greatly simplify the pre-processing stage. For this feature a good quality body-fitted surface mesh has to be provided. The volume mesher has several tools for local refinement and boundary layer meshing as well as for shell (non-body-fitted) meshes. In the cases where FSI simulations result in large displacements the solver could automatically re-mesh to keep an acceptable mesh quality. For the case where error control is activated the mesher may automatically refine or coarse according to the error measures.

Other possibilities include the solution of free surface flows and multi-fluid simulation, flows at high Reynolds number where turbulence effects are important and the coupling with a thermo-mechanics solver for conjugate heat transfer applications.

The present analysis is a purely CFD application where the full Navier-Stokes equations are solved. The meshes in all cases are built by the solver with the objective of studying the drag force over bluff bodies. In the following section we will present the results obtained for the Ahmed body problem.

# 2 Flow around the Ahmed body

## 2.1 Problem description

Ground vehicles can be termed as bluff bodies that move close to the road surface and fully submerged in its surrounding fluid. In general, for the more usual commercial passenger cars, buses and trucks, compressible effects can be neglected and an incompressible viscous fluid model can be assumed. The high Reynolds number based on the vehicle length results in a flow at a fully turbulent regime.

The Ahmed body [1] is a very simplified geometry with no accessories or wheels. It is frequently employed as a benchmark in vehicle aerodynamics since it retains most of the primary behavior of the vehicle aerodynamics. A sketch of the geometry is represented in Fig. 1 where L = 1044 [mm] and the height $H$ and the width $B$ are defined according to the following ratio: $(L : B : H) = (1 : 0.373 : 0.276)$.

The analysis is usually focused on the flow in the near wake and the variation of drag with the rear slant angle $\alpha$. The main challenge in the numerical simulation of the Ahmed body is to accurately predict the drag and lift coefficients at high Reynolds numbers. Fig. 2 shows the plot obtained by Ahmed

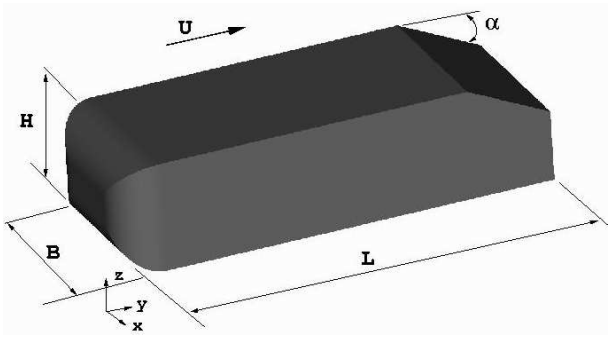


Figure 1: Schematic representation of Ahmed body

and al. [1] from experimental observations. For this analysis the angle values of $\alpha = 12.5^o$ and $\alpha = 28^o$ will be studied as they both correspond to two critical slant angle values, one to the minimum of drag, the other close to the so-called "drag crisis".

## 2.2 Computational domain

The fluid domain used in the CFD simulation is shown in Fig. 3. The volume mesh consists of 1660315 tetrahedral elements and 297248 nodes. To capture the effects of the flow in the area close to the surface several layers of anisotropic elements were introduced. Some snapshots of the mesh are depicted in Fig. 4. An interior boundary (see Fig. 3) was used to specify the mesh size inside the domain.

## 2.3 Fluid parameters

The fluid parameters were set to be air at $15^o$C where its kinematic viscosity is $\nu = 14.75 \times 10^6 [m^2/s]$. A uniform inflow velocity was set to $U_\infty = 60 m/s$. Taking the characteristic length as the length of the Ahmed body we obtain a Reynolds number $R = 4.25 \times 10^6$.

## 2.4 Choice of the turbulence model

In the case of flows at high Reynolds number the choice of the turbulence model is crucial in order to correctly reproduce vortexes, boundary layer laminar to turbulent transitions and other turbulent three dimensional behaviors.

### 2.4.1 The RANS model

The RANS equations determine mean flow quantities but they require turbulence models to close them. These equations are provided by the different RANS

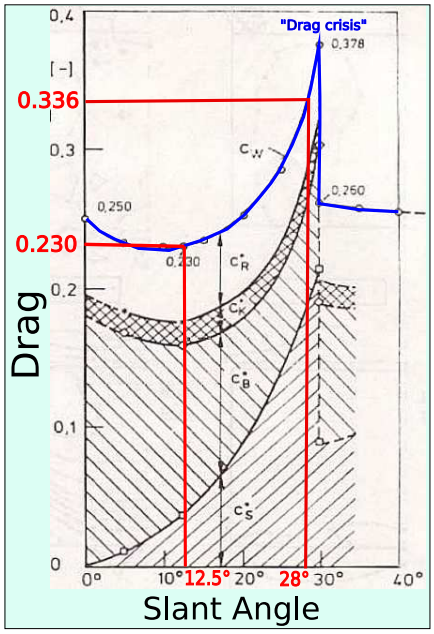


Figure 2: Experimental curve of drag coefficient (in Blue) vs. slant angle

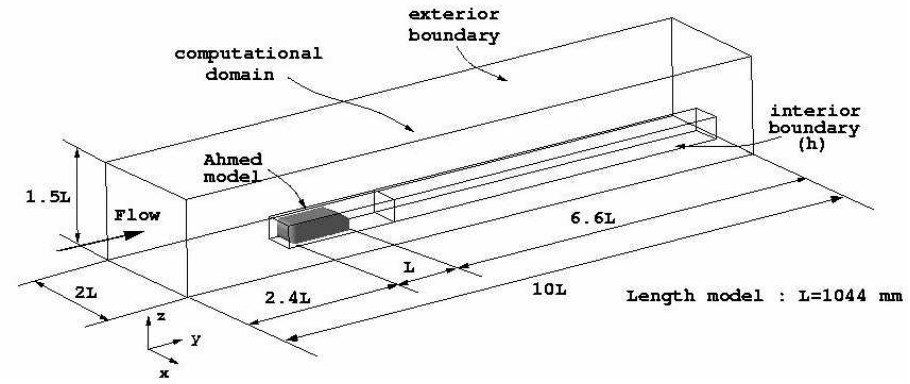


Figure 3: CFD domain for the Ahmed body problem.

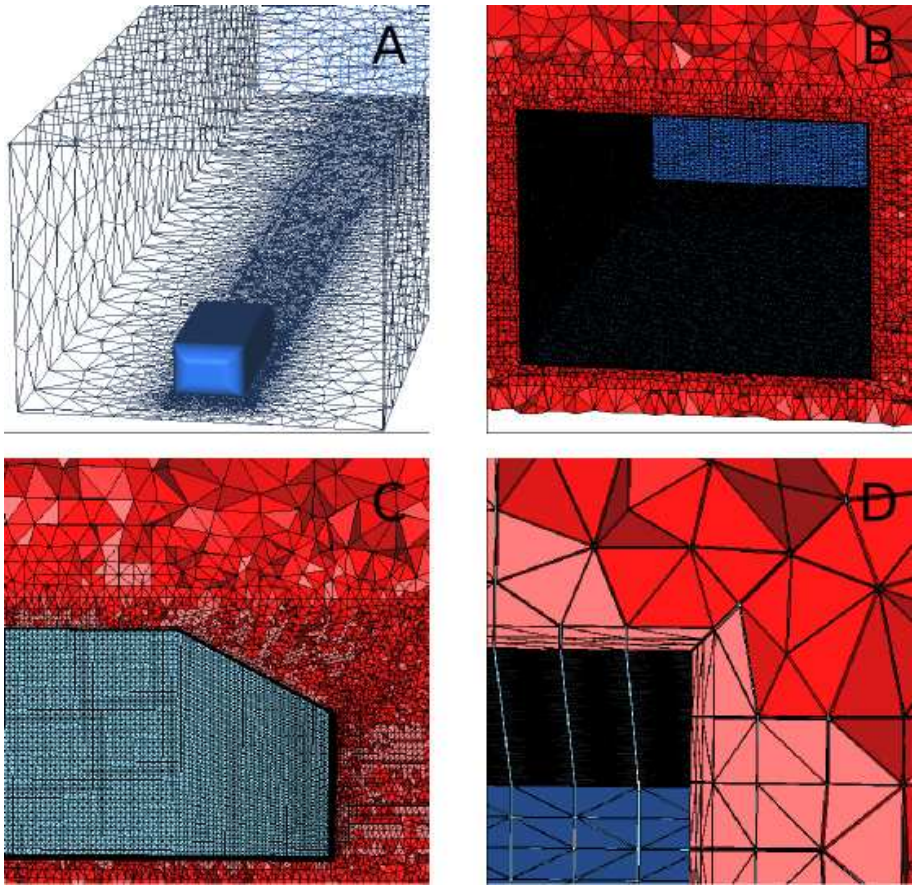


Figure 4: Mesh used in the Ahmed body problem. “A” shows the surface mesh. “B” is a transverse cut. “C” shows the mesh in the slant angle area. “D” shows the boundary layer mesh close to the surface.

models assuming different hypothesis on the flow. The incompressible solver provides a $k-\epsilon$ model which is one of the most widely used turbulence models in CFD. However, it has been shown that RANS models can perform either relatively well or poorly according to the slant angle [2]. One explanation is that most RANS models often miss the flow separation at the rear part for such slant angles and fail to correctly predict the behavior of massively separated flows. For this analysis, we will therefore focus on an other turbulence model provided by the solver: the LES approach.

### 2.4.2 The LES model

As the power of computer increases LES models have become a popular technique in order to simulate turbulence. Those models are based on the assumption that large eddies contain most of the kinetic energy of the flow and depend on the geometry while the smaller ones are considered more universal and independent of the flow's geometry. Therefore LES models will apply a filter on the flow directly solving large eddies while simulating smaller ones. For our analysis, the LES Smagorinsky model available in the solver will be chosen.

## 2.5 Numerical results

### 2.5.1 Flow in the near wake

For the $\alpha = 12.5^o$ case, Fig. 5 shows the instantaneous velocity streamlines on the symmetrical plane y=0 which confirm the good behavior of the flow. It can be observed that the flow remains attached over the whole slant as expected while two main vortexes are formed in the near wake of the Ahmed body. However, for the $\alpha = 28^o$ case, the flow separation over the slant results in an increase of the drag which can be clearly identified on Fig. 6.

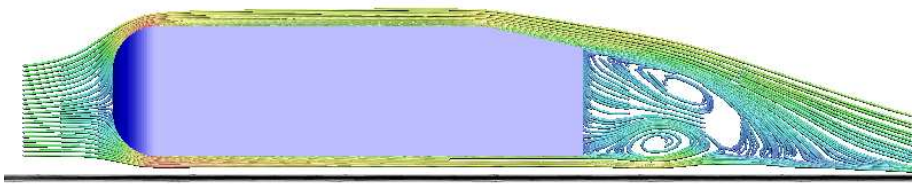

Figure 5: Velocity streamlines on the symmetrical plane y=0 for the $\alpha = 12.5^o$ case.

Fig. 7 shows an example of the flow's separation on the Ahmed body side resulting in two trailing vortexes for the $\alpha = 12.5^o$ case . Fig. 8 shows the isobars in the y=0 symmetric plane for the $\alpha = 12.5^o$ case where the local depression bubble happening at the beginning of the slant can be observed.

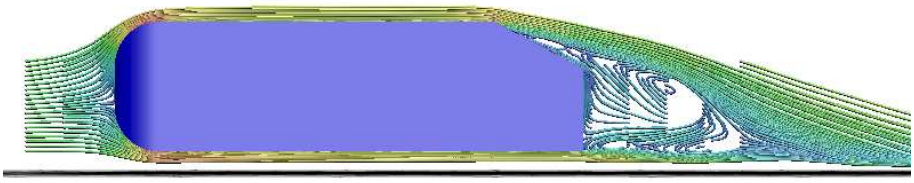

Figure 6: Velocity streamlines on the symmetrical plane y=0 for the $\alpha = 28^o$ case.

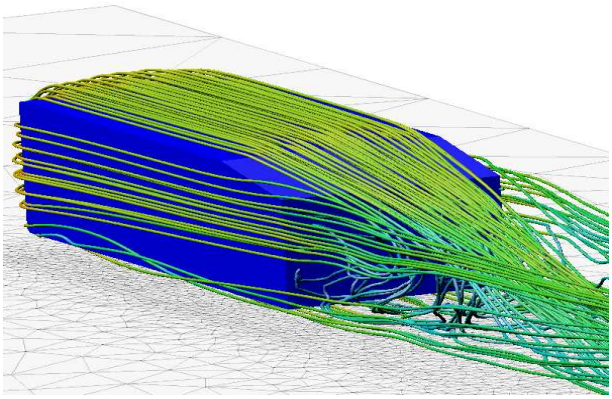

Figure 7: Velocity streamlines over the Ahmed body for the $\alpha = 12.5^o$ case.

### 2.5.2 Drag coefficient

For this analysis we will focus on the drag value and compare the computed results to the experimental ones.

The drag coefficient ($C_D$) is computed as $C_D = 2F_D/\rho U_\infty^2 A_{proj}$ where $F_D$ is the drag force, $U_\infty$ is the non-perturbed velocity, $\rho$ is the fluid density and $A_{proj}$ is the projected area of the vehicle.

The resulting drag and time average drag coefficients obtained from the numerical simulation using LS-DYNA incompressible CFD solver are shown in Fig. 9 and Fig. 10 . For the $\alpha = 12.5^o$ case, once the steady state has been reached, the time average drag is $C_D = 0.232$ which is in very good agreement with the experimental value of $C_D = 0.230$. The error obtained from the simulation is $\varepsilon = +0.86\%$. For the $\alpha = 28^o$ case, the time average drag is $C_D = 0.319$ which

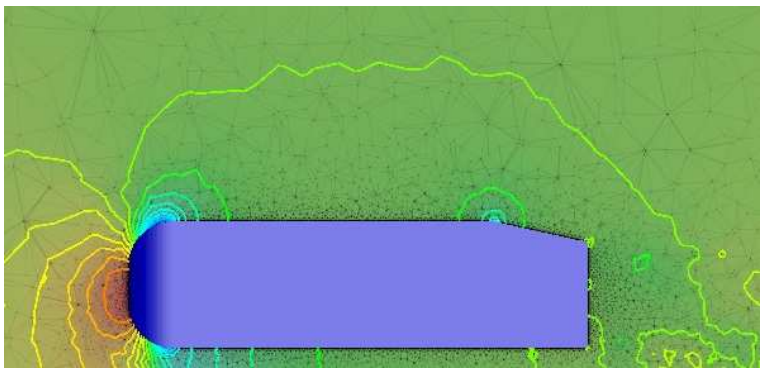

Figure 8: Isobars on the symmetrical plane y=0 for the $\alpha = 12.5^o$ case.

is also still in good agreement with the experimental value of $C_D = 0.336$. The error obtained from the simulation is $\varepsilon = -5.06\%$.

### 2.6 Other possible applications of LS-DYNA in the aerodynamics study of bluff bodies

When using the incompressible CFD solver in LS-DYNA, the user can also access all of LS-DYNA solid mechanics capabilities. In this way, coupling between fluid and solid parts is greatly simplified making it a very good tools for problems involving fluid structure interactions. For example, in the context of aerodynamic design, the analysis of suspension systems integrated to the aerodynamic analysis of the vehicle may be of interest. A set of springs and dumpers may be attached to the vehicle to study the dynamic response of the suspension under the aerodynamic loads.

## References


[1] S. Ahmed, G. Ramm, and G. Faltin. Some salient features of the time-averaged ground vehicle wake. *SAE paper*, 840300:1–31, 1984.

[2] M. Storti ad J. D'Elia G. Franck, N. Nigro. Numerical simulation of the ahmed vehicle model near wake.

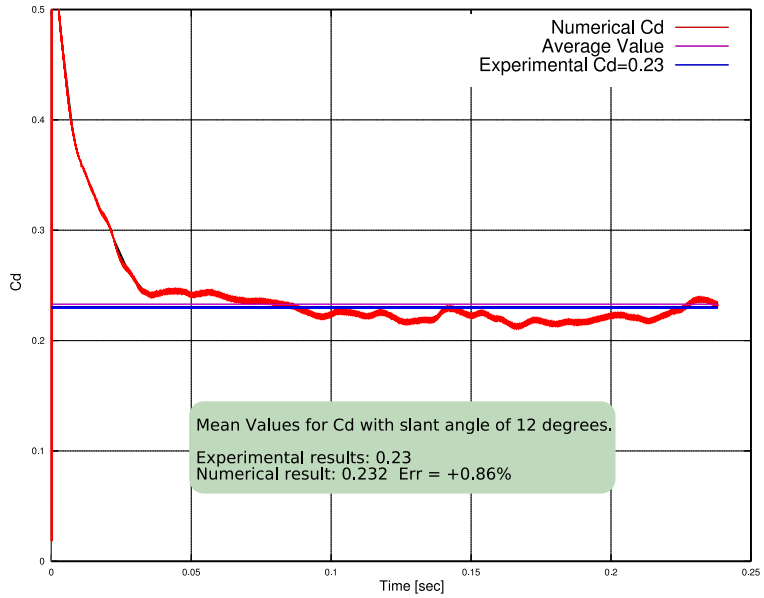


Figure 9: Drag plot as a function of the iteration number for the $\alpha = 12.5^o$ case
.

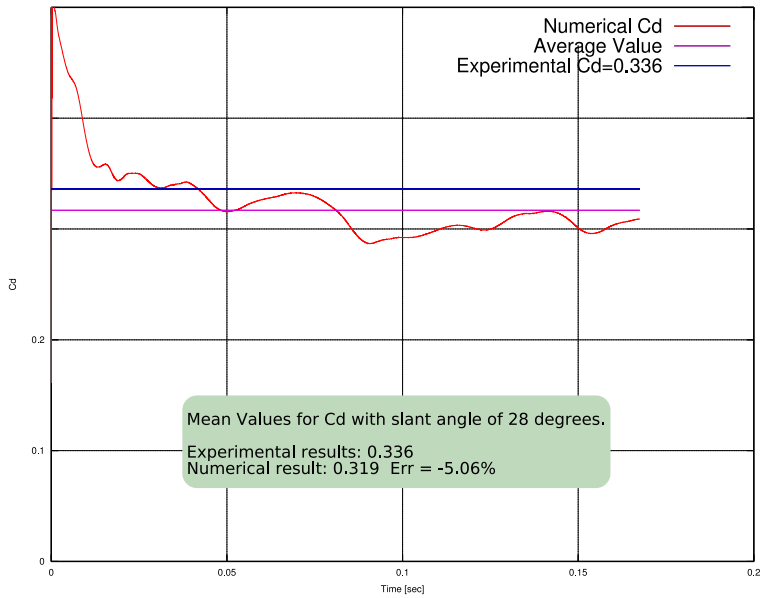


Figure 10: Drag plot as a function of the iteration number for the $\alpha = 28^o$ case.